

**This item is the archived peer-reviewed author-version of:**

Global trends in carbon sinks and their relationships with  $CO_2$  and temperature

**Reference:**

Fernandez-Martinez Marcos, Sardans J., Chevallier F., Ciais P., Obersteiner M., Vicca Sara, Canadell J.G., Bastos A., Friedlingstein P., Sitch S., ....- Global trends in carbon sinks and their relationships with  $CO_2$  and temperature  
Nature climate change - ISSN 1758-678X - 9:1(2019), p. 73-79  
Full text (Publisher's DOI): <https://doi.org/10.1038/S41558-018-0367-7>  
To cite this reference: <https://hdl.handle.net/10067/1556810151162165141>

1 **Global trends in carbon sinks and their relationships with CO<sub>2</sub> and**  
2 **temperature**

3 **Authors:** M. Fernández-Martínez<sup>\*1</sup>, J. Sardans<sup>2,3</sup>, F. Chevallier<sup>4</sup>, P. Ciais<sup>4</sup>, M. Obersteiner<sup>5</sup>, S.  
4 Vicca<sup>1</sup>, J. G. Canadell<sup>6</sup>, A. Bastos<sup>4</sup>, P. Friedlingstein<sup>7</sup>, S. Sitch<sup>7</sup>, S.L. Piao<sup>8,9</sup>, I.A. Janssens<sup>1</sup>, J.  
5 Peñuelas<sup>2,3</sup>.

6 **Affiliations:**

7 <sup>1</sup> Centre of Excellence PLECO (Plant and Vegetation Ecology), Department of Biology, University  
8 of Antwerp, 2610 Wilrijk, Belgium.

9 <sup>2</sup> CSIC, Global Ecology Unit, CREAM-CSIC-UAB, Cerdanyola del Vallès, 08193 Barcelona,  
10 Catalonia, Spain

11 <sup>3</sup> CREAM, Cerdanyola del Vallès, 08193 Barcelona, Catalonia, Spain

12 <sup>4</sup> Laboratoire des Sciences du Climat et de l'Environnement, CEA CNRS UVSQ, 91191 Gif-sur-  
13 Yvette, France

14 <sup>5</sup> International Institute for Applied Systems Analysis, Schlossplatz 1, 2361 Laxenburg, Austria

15 <sup>6</sup> Global Carbon Project, CSIRO Oceans and Atmosphere, Canberra, ACT 2601, Australia

16 <sup>7</sup> College of Engineering, Computing and Mathematics, University of Exeter, Exeter EX4 4QF, UK

17 <sup>8</sup>Sino-French Institute of Earth System Sciences, College of Urban and Environmental Sciences,  
18 Peking University, Beijing 100871, China

19 <sup>9</sup> Institute of Tibetan Plateau Research, Chinese Academy of Sciences, Beijing 100085, China

20 \*Correspondence to: M. Fernández-Martínez, marcos.fernandez-martinez@uantwerpen.be

21

22

23 Elevated CO<sub>2</sub> increases photosynthesis and, potentially, net ecosystem production  
24 (NEP) meaning greater CO<sub>2</sub> uptake. Climate, nutrients, and ecosystem structure,  
25 however, influence the effect of increasing CO<sub>2</sub>. Here, we analysed global NEP from  
26 MACC-II and Jena CarboScope atmospheric-inversions and 10 dynamic global  
27 vegetation models (TRENDY), using statistical models to attribute the trends in NEP to  
28 its potential drivers: CO<sub>2</sub>, climatic variables and land-use change. We find that increasing  
29 CO<sub>2</sub> was consistently associated with increased NEP (1995-2014). Conversely,  
30 increasing temperatures were negatively associated with NEP. Using the two  
31 atmospheric inversions and TRENDY, the estimated global sensitivities for CO<sub>2</sub> were  $6.0$   
32  $\pm 0.1$ ,  $8.1 \pm 0.3$  and  $3.1 \pm 0.1$  Pg C per 100 ppm ( $\sim 1$  °C increase), and  $-0.5 \pm 0.2$ ,  $-0.9 \pm$   
33  $0.4$  and  $-1.1 \pm 0.1$  Pg C °C<sup>-1</sup> for temperature. These results indicate a positive CO<sub>2</sub> effect  
34 on terrestrial C sinks that is constrained by climate warming.

35

36 In recent decades, terrestrial ecosystems have been absorbing 15–30% of all  
37 anthropogenic CO<sub>2</sub> emissions<sup>1,2</sup>. Direct and indirect anthropogenic impacts on the  
38 biosphere, however, can alter terrestrial sinks in the short and long terms<sup>3–6</sup>. Identifying  
39 the factors that affect the capacity of the biosphere to absorb carbon (C) and quantifying  
40 the magnitude of the sensitivity of this C sink to its driving factors helps to increase  
41 confidence in future projections of the coupled C cycle/climate system.

42 Increasing plant growth is a robust response to increasing CO<sub>2</sub> concentrations under  
43 experimental conditions (CO<sub>2</sub> fertilization effect)<sup>7,8</sup>. The extent to which increases in CO<sub>2</sub>  
44 can enhance large-scale photosynthesis and ultimately net ecosystem production (NEP)  
45 remains uncertain<sup>5,7</sup>. Detecting this effect in the real world is much more difficult than  
46 under controlled experiments. However, recent efforts using eddy-covariance-based  
47 data and statistical models have been successful in detecting positive effects of CO<sub>2</sub> on  
48 water-use efficiency (WUE)<sup>9</sup>, photosynthesis, and NEP<sup>5</sup>.

49 The potential positive effect of elevated CO<sub>2</sub> on productivity could be influenced by global  
50 warming<sup>6</sup> and altered precipitation patterns<sup>10</sup> since both water availability and  
51 temperature are strong drivers of photosynthesis and respiration worldwide<sup>11–13</sup>. Land-  
52 use change also alters the capacity of the biosphere to sequester C because land use  
53 causes a drastic change in C turnover and productivity. Atmospheric deposition of  
54 nitrogen (N) and sulphur (S) from the use of fossil fuels and fertilisers may also alter  
55 ecosystem biodiversity, function, productivity and NEP<sup>5,14–17</sup>. N deposition is usually  
56 positively correlated with ecosystem productivity and NEP<sup>17–19</sup>. Conversely, S deposition  
57 may reduce ecosystem carbon sinks, this has rarely been investigated in field studies<sup>20,21</sup>  
58 and absent from global models. Soil acidification, caused by acid deposition, of N and S,  
59 often decreases the availability of soil nutrients<sup>22</sup> and potentially reduces NEP<sup>23</sup>.

60 The observations underlying the driver analysis of NEP described above were largely  
61 limited to temperate and boreal study sites, making it difficult to assess global scalability.  
62 Additionally, until recently, the only way to assess terrestrial C sink was from ensembles  
63 of dynamic global vegetation models (DGVMs) or as a residual sink, by subtracting  
64 atmospheric and ocean sinks to the estimates of CO<sub>2</sub> emissions. Currently, inversion  
65 models, as well as long-term remotely sensed data<sup>24</sup>, can be used to test the generality  
66 of the patterns derived from ground-based measurements. Inversion models provide  
67 continuous gridded estimates for the net flux of land-atmosphere CO<sub>2</sub> exchange (i.e.  
68 NEP) with global coverage<sup>25,26</sup>. The gridded NEP results from inversions, combined with  
69 CO<sub>2</sub>-concentration records, gridded fields for climate, land-use change, and atmospheric  
70 deposition, are arguably the best observation-based data to attempt a first empirical

71 study of the combined effects of CO<sub>2</sub>, changes in climate and land use, and atmospheric  
72 N and S deposition on terrestrial NEP patterns at the global scale. Given that previous  
73 site level studies revealed that increasing CO<sub>2</sub> is a dominant driver of trends in NEP, we  
74 expect that it will also be the dominant driver at larger spatial scales and across the  
75 globe.

76 Here we investigate if the trends of NEP from the two most widely used multi-decadal  
77 inversion models (MACC-II and Jena CarboScope) and DGVMs (TRENDY) from 1995  
78 to 2014 are related to increasing atmospheric CO<sub>2</sub> and changing climate (temperature,  
79 precipitation, and drought). Additionally, the effect of land-use on NEP at the global scale  
80 was investigated using statistical models to assess the sensitivity of NEP to the  
81 abovementioned predictors. We also analysed the effect of changing rates of  
82 atmospheric deposition of oxidised and reduced N and S on NEP, combined with  
83 increasing CO<sub>2</sub> and changing climate and land use, over Europe and the USA.

#### 84 *CO<sub>2</sub> and climate effects on global NEP*

85 Global land (excluding Antarctica) mean annual NEP was  $2.3 \pm 0.9$ ,  $2.3 \pm 1.5$  and  $1.6 \pm$   
86  $0.5 \text{ Pg C y}^{-1}$  (mean  $\pm 1\sigma$ ), respectively, for MACC-II, Jena CarboScope and the TRENDY  
87 ensemble during the period 1995–2014, similar in magnitude to the recent global carbon  
88 budget<sup>2</sup>. Both inversions and the TRENDY ensemble showed an overall positive trend  
89 in NEP from 1995 to 2014. The estimated NEP increased by (mean  $\pm 1\text{SE}$ )  $116.9 \pm 6.1$   
90  $\text{Tg C y}^{-1}$  for the MACC-II dataset, by  $178.0 \pm 8.1 \text{ Tg C y}^{-1}$  for the Jena CarboScope  
91 dataset, and by  $22.5 \pm 3.1 \text{ Tg C y}^{-1}$  for the TRENDY ensemble (**Figure 1**). This supports  
92 the increases in the global carbon budget<sup>2</sup>, with a lower increase of the DGVMs than  
93 those shown by the inversion models. The large differences between inversion models  
94 and DGVMs may arise because of the lack of information on river fluxes, inadequate  
95 parameterisations concerning land management and degradation in the process models  
96 or because of potential biases in inversion models. Both inversion model datasets  
97 produced similar trends for many parts of the world, an increasing NEP for Siberia, Asia,  
98 Oceania, and South America, and a decreasing NEP for the southern latitudes of Africa.  
99 Differences between inversions emerged for Europe and North America, possibly  
100 because Jena CarboScope inversion uses a larger spatial error correlation of prior fluxes  
101 than MACC-II or because of other inversion settings<sup>2</sup>. However, their different flux priors  
102 did not drive differences in the trends between both datasets, given that priors did not  
103 change over the studied period. Jena CarboScope showed largely positive trends for  
104 Europe and largely negative trends for North America; MACC II showed more variation  
105 in the trends for both continents. The trends identified by the TRENDY ensemble agreed

106 with atmospheric inversions for the northernmost latitudes, indicating an increase in C-  
107 sink capacity, but differed from those in many other regions.

108 Our analyses on temporal contributions, using the temporal anomalies of our predictors,  
109 attributed the increases in global NEP to increasing CO<sub>2</sub> but found a consistent negative  
110 impact of temperature on NEP, which limited the positive effect of increasing CO<sub>2</sub> (**Figure**  
111 **1**). These results were consistent for both datasets and most of the DGVMs of the  
112 TRENDY ensemble. The predictors used in this study explained a modest proportion of  
113 the variance in NEP, in contrast to the variance explained by spatial variability (i.e., the  
114 pixel), which was rather high (**Supplementary Information (SI), Section 2**). Unknown  
115 contributions to trends in NEP, the difference between all contributions and the observed  
116 trend, were very close to zero for the analyses on inverse models and the TRENDY  
117 ensemble (**Figure 1**). This result suggests that trends were very well captured by our  
118 analyses, indicating that the methodology was able to disentangle spatial from temporal  
119 variability. The sensitivity of NEP to increasing CO<sub>2</sub> averaged  $0.45 \pm 0.01$ ,  $0.61 \pm 0.03$   
120 and  $0.23 \pm 0.01$  g C m<sup>-2</sup> ppm<sup>-1</sup> for MACC-II, Jena CarboScope and TRENDY, respectively  
121 (**Table 1**), representing sensitivities over the entire terrestrial surface of  $60.4 \pm 1.2$ ,  $81.4$   
122  $\pm 3.4$  and  $30.7 \pm 1.2$  Tg C ppm<sup>-1</sup>, respectively. Despite lower temporal attributions for  
123 temperature than CO<sub>2</sub>, the sensitivity of NEP to temperature was high, at  $-3.8 \pm 1.1$ ,  $-6.4$   
124  $\pm 2.9$  and  $-8.1 \pm 0.9$  g C m<sup>-2</sup> y<sup>-1</sup> °C<sup>-1</sup> for the MACC-II, Jena CarboScope and TRENDY  
125 models, respectively, equivalent to global sensitivities of  $-515.7 \pm 152.4$ ,  $-859.2 \pm 386.3$   
126 and  $-1088.0 \pm 118.1$  Tg C °C<sup>-1</sup>, respectively. Trends in NEP and the effect of CO<sub>2</sub> and  
127 temperature on NEP significantly differed in magnitude amongst the datasets used,  
128 however, they all point towards the same conclusion: global NEP has increased during  
129 the study period and increasing CO<sub>2</sub> has been the most likely driving factor despite  
130 increasing temperatures constraining this positive effect. The exact magnitude of the  
131 effect of increasing CO<sub>2</sub> and temperatures on global carbon cycle remains to be  
132 established

### 133 *Spatial variability on CO<sub>2</sub> and climate change effects on NEP*

134 Our statistical models for the MACC-II and Jena CarboScope datasets indicated that the  
135 positive effect of CO<sub>2</sub> on NEP was higher in regions with higher annual precipitation and  
136 that this positive effect increased with increasing temperatures (**Figure 2, SI Section**  
137 **1.1**). In contrast, our analyses using the TRENDY ensemble did not show a significant  
138 interaction between CO<sub>2</sub> and precipitation or with temperature, highlighting the different  
139 behaviour in the DGVMs compared to inversion models. We also found a significant  
140 positive interaction between mean annual temperature and CO<sub>2</sub> for Jena CarboScope

141 and TRENDY. However, the same interaction was negative for MACC-II. On the other  
142 hand, increasing temperatures reduced NEP in warm regions but increased NEP in cold  
143 regions (**Figure 2**).

144 The analyses on temporal contributions performed for inversion and TRENDY NEP  
145 averaged over latitudinal bands (boreal, >55°; temperate, 35-55°; subtropical, 15-35°;  
146 and tropical, 15°N-15°S), further supported previous results obtained at the global scale  
147 (**Table 2, SI Sections 2.2–2.7**). Increasing CO<sub>2</sub> was the main factor accounting for  
148 increasing trends in NEP, with a consistent positive temporal contribution for almost all  
149 latitudinal bands considered and for all three datasets. However, contributions estimated  
150 from the TRENDY ensemble were generally lower than those of the inversion models.  
151 Proportionally, increasing CO<sub>2</sub> accounted for more than 90% of the trends in NEP in  
152 MACC-II and Jena CarboScope datasets. For the TRENDY ensemble, the estimated  
153 contribution of CO<sub>2</sub> to the trends in global NEP was more than 2.7 times higher than the  
154 estimated trends. Increasing temperatures had a negative effect for all latitudinal bands  
155 for the inversion models, but most effects were not statistically significant and need to be  
156 interpreted as such. Instead, our analyses for the TRENDY ensemble indicated a  
157 significant negative effect for all latitudinal bands, except for the temperate southern  
158 hemisphere. Similarly, the proportional contribution of temperature to the trends in NEP  
159 was less than 10% for the inversion models, but accounted for almost 95% of the trends  
160 estimated using the TRENDY ensemble. These results suggest that the  
161 parameterisation of temperature in the DGVMs does not accurately reproduce the  
162 estimation of the inverse models.

163 Despite all regions presented, on average, positive trends, the tropical regions clearly  
164 had the highest contribution, across all three datasets, to global NEP trends accounting  
165 for almost half of the increase (**Table 2**). Similarly, the tropical regions had the highest  
166 sensitivity to CO<sub>2</sub> increase, accounting for more than half of the total global sensitivity  
167 (**Table 1**). A similar pattern was found for temperature, although the sign of the  
168 contribution was positive for MACC-II but negative for Jena CarboScope and TRENDY.  
169 The contribution of the southern hemisphere to the global trends was very modest  
170 compared to the contribution of the northern hemisphere using all datasets. Our results  
171 using the MACC-II dataset showed that subtropical, temperate and boreal regions of the  
172 northern hemisphere accounted for 44.2% of the global trends in NEP, while only 9.5%  
173 was attributed to subtropical and temperate regions of the southern hemisphere. Using  
174 the Jena CarboScope dataset these regions accounted for 63.3% and 6.1%,  
175 respectively. Differences on the regional attributions between inversion models may  
176 emerge from the different interhemispheric transport models or other inversion settings<sup>2</sup>.

177 Results from the TRENDY ensemble were more extreme, because they indicated a  
178 negative contribution of the subtropical and temperate regions to the global trends in  
179 NEP. Differences between the global estimates (trends and contributions of CO<sub>2</sub> and  
180 temperature) and the sum of every region were low for all datasets. Contribution of other  
181 variables to the trends in NEP (precipitation, drought, land-use change, and unknown  
182 variables) were on average also low for most of the latitudinal bands, despite the  
183 variability amongst datasets (**Table 2**).

#### 184 *Atmospheric deposition*

185 The MACC-II and Jena CarboScope datasets showed that NEP increased over Europe  
186 and the USA by  $0.45 \pm 0.13$  and  $0.68 \pm 0.16$  g C m<sup>-2</sup> y<sup>-1</sup>, respectively (**Figure S1**). Our  
187 temporal contribution analyses suggested that increasing atmospheric CO<sub>2</sub> in both  
188 datasets contributed significantly to increasing NEP. NEP sensitivity to CO<sub>2</sub> was more  
189 than two-fold higher in the Jena CarboScope than the MACC-II dataset (**Table S1**),  
190 similar to the temporal contributions, at  $0.22 \pm 0.06$  and  $0.46 \pm 0.07$  g C m<sup>-2</sup> y<sup>-1</sup> ppm<sup>-1</sup> for  
191 the MACC-II and Jena CarboScope models, respectively. The temporal contribution of  
192 decreasing N<sub>OX</sub> deposition to NEP differed between the two datasets; the contribution  
193 was positive for MACC-II and negative for Jena CarboScope. Our analyses consequently  
194 estimated a negative sensitivity of NEP to N<sub>OX</sub> for the MACC-II dataset but a positive  
195 sensitivity for the Jena CarboScope dataset. Additionally, neither MACC-II, nor Jena  
196 CarboScope indicated a strong impact of land use change.

197 These statistical models indicated that, in both datasets, the positive effect of CO<sub>2</sub> on  
198 NEP was higher in regions with higher N<sub>RED</sub> deposition but lower in regions with high S  
199 deposition (means for MACC-II and annual anomalies for Jena CarboScope; see **SI**  
200 **section 2.8**). The results for N<sub>OX</sub> deposition, however, differed between the models. The  
201 positive effect of CO<sub>2</sub> on NEP for the MACC-II dataset was constrained by the annual  
202 anomalies of N<sub>OX</sub> but was higher for the Jena CarboScope dataset. We also estimated  
203 an overall negative but not significant sensitivity of NEP to S deposition for both inversion  
204 models.

#### 205 *CO<sub>2</sub> fertilisation and global NEP*

206 The positive effect of atmospheric CO<sub>2</sub> on NEP must originate from a stronger positive  
207 effect on photosynthesis than on the sum of all respiratory processes. Increasing  
208 atmospheric CO<sub>2</sub> concentrations have been widely reported to increase ecosystem  
209 photosynthesis, mainly by two mechanisms: i) increasing carboxylation rates and  
210 decreasing photorespiration<sup>27</sup>, and ii) decreasing stomatal conductance and therefore

211 increasing WUE<sup>9,28</sup>, which would theoretically increase photosynthesis under water  
212 limitation. An increase in GPP by either mechanism may thus account for the higher NEP  
213 due to increasing atmospheric CO<sub>2</sub>. A recent global analysis suggested that most of the  
214 GPP gains from CO<sub>2</sub> fertilization are associated with ecosystem WUE<sup>29</sup>. The positive  
215 interaction between CO<sub>2</sub> and annual precipitation that we found may not support this  
216 hypothesis (**Figure 2**), given that plants living under wet conditions are usually less  
217 efficient in water use. However, plants having higher water availability may benefit from  
218 increasing CO<sub>2</sub> more than those suffering drought because photosynthesis would not be  
219 water-limited.

220 Our estimates of global NEP sensitivity to CO<sub>2</sub> were  $0.45 \pm 0.01$ ,  $0.61 \pm 0.03$  and  $0.23 \pm$   
221  $0.01 \text{ g C m}^{-2} \text{ ppm}^{-1}$  (globally  $60.4 \pm 1.2$ ,  $81.4 \pm 3.4$  and  $30.7 \pm 3.4 \text{ Tg C ppm}^{-1}$ ) for the  
222 MACC-II, Jena CarboScope and TRENDY datasets, respectively, but these estimates  
223 varied amongst the latitudinal bands and were inconsistent between datasets (**Table 1**).  
224 These estimates were similar to those reported in CO<sub>2</sub>-enrichment FACE experiments<sup>30</sup>,  
225 despite the fact that FACE values were calculated for a much higher CO<sub>2</sub> range for which  
226 the effect of CO<sub>2</sub> may saturate<sup>31</sup>. However, they were much lower than the  $4.81 \pm 0.52 \text{ g}$   
227  $\text{C m}^{-2} \text{ ppm}^{-1}$  reported in a study using eddy-covariance flux towers for a similar period<sup>5</sup>.  
228 The much larger areas analysed by the inverse models than the footprints covered by  
229 the eddy-covariance flux towers, and FACE experiments, may explain these differences  
230 between the estimates. Flux towers are usually located in relatively homogenous,  
231 undisturbed ecosystems, while each pixel in the inverse model aggregates information  
232 from several ecosystems (and even biomes), often including non-productive land such  
233 as bare soil or cities.

234 Our results indicated that the variability of the estimates of NEP sensitivity to CO<sub>2</sub>  
235 amongst the latitudinal bands might be associated with differences in climate and  
236 atmospheric N and S deposition. The two atmospheric inversion models indicated that  
237 the effect of CO<sub>2</sub> fertilisation was stronger in wet climates (high annual precipitation)  
238 (**Figure 2**), supporting the estimates provided by the latitudinal bands, with the highest  
239 sensitivity estimates for the tropical band (**Table 1**). However, analyses based on the  
240 TRENDY ensemble did not show the same results. The positive effect of CO<sub>2</sub> tended to  
241 increase with temperature anomalies in both inversion models, but, again, the DGVMs  
242 did not show the same behaviour. These differences between inversion models and  
243 process-based models suggest that DGVMs still fail to capture some of the interactions  
244 occurring in nature. The MACC-II and Jena CarboScope datasets further agreed on a  
245 stronger positive effect of increasing CO<sub>2</sub> in regions with higher N<sub>RED</sub> deposition, which

246 confirms previous studies suggesting that the effect of CO<sub>2</sub> fertilisation is stronger in  
247 nitrogen-rich sites<sup>32–34</sup>.

#### 248 *Climate, land-use and C sinks*

249 Climatic warming clearly had a secondary effect on the trends in NEP from 1995 to 2014.  
250 The MACC-II, Jena CarboScope and TRENDY datasets estimated that NEP decreased  
251 globally by around  $-0.5 \pm 0.2$ ,  $-0.9 \pm 0.4$  and  $-1.1 \pm 0.1$  Pg C for every degree of increase  
252 in the Earth's temperature. Assuming that a CO<sub>2</sub> increase of 100 ppm is equivalent to an  
253 increase of global temperature of 1 °C, the effect of the increasing CO<sub>2</sub> concentrations  
254 largely outweighs the negative effect of increasing temperature on NEP (global  
255 estimates:  $6.0 \pm 0.1$ ,  $8.1 \pm 0.3$  and  $3.1 \pm 0.1$  Pg C for a 100 ppm of CO<sub>2</sub> increase  
256 according to MACC-II, Jena CarboScope and TRENDY). The difference, though, is much  
257 lower for TRENDY than for the inversion models, having a higher negative impact of  
258 temperature and a lower positive effect of CO<sub>2</sub>. This difference in the effects of  
259 temperature and CO<sub>2</sub> may explain the lower trends observed in TRENDY datasets  
260 compared to MACC-II and Jena CarboScope. It also suggests that a different  
261 parameterisation of temperature, CO<sub>2</sub> and their interaction may be needed on DGVMs  
262 to capture the observed trends in the inversion models.

263 The quasi monotonically increasing atmospheric CO<sub>2</sub> concentrations have been more  
264 important than temperature in driving NEP trends. Increasing temperature, however, did  
265 not have the same effect on NEP around the world. The analyses of both inverse models  
266 indicated that increasing temperatures had a positive effect on NEP only in cold regions  
267 (when MAT  $\leq 1.5$ , 9 and  $-5.9$  °C for MACC-II and Jena CarboScope and TRENDY  
268 respectively, when CO<sub>2</sub> = 400 ppm, see **SI section 2.1**, and **Figure 2**). These findings  
269 support previous literature reporting a positive effect between temperature increase and  
270 NEP in temperate and boreal forests<sup>35</sup>. Instead, the general negative effect of  
271 temperature on NEP could be due to a greater stimulation of Re than photosynthesis by  
272 higher temperatures<sup>36,37</sup>. The potential benefit to C sequestration of increased  
273 photosynthesis would then be negated by a greater increase in Re. Increasing  
274 temperatures can also be linked to heat waves and drier conditions, which may decrease  
275 GPP more than Re<sup>38</sup>.

276 The effects of land-use change on NEP trends differed greatly amongst the datasets,  
277 both at the global scale and when using latitudinal bands. Our statistical models identified  
278 several significant relationships between NEP and land-use change, but the large  
279 differences in effects (direction and magnitude) amongst the datasets preclude drawing

280 firm conclusions. The coarse resolution of analysis likely blurred the effects of land-use  
281 change on the NEP trends.

282 Our study highlights the dominant role of rising atmospheric CO<sub>2</sub> concentrations  
283 triggering an increase in land C sinks over the entire planet from 1995 to 2014, with the  
284 tropics accounting for around half of this increase in NEP despite being only around 22%  
285 of the global land (excluding Antarctica, **Table 2**). Therefore, preserving tropical  
286 ecosystems should be a global priority in order to mitigate anthropogenic CO<sub>2</sub> emissions.  
287 Temperature has diminished the capacity of terrestrial ecosystems to sequester C, which  
288 jeopardises future C sink capacity in light of global warming. So far, our results suggest  
289 that the benefit of increasing atmospheric concentrations of CO<sub>2</sub> are still compensating  
290 the negative ones of temperature rise, in terms of C sequestration. However, if it has not  
291 started to change already<sup>6</sup>, this pattern may eventually reverse with saturation of land C  
292 sinks<sup>5,31</sup> or because warm ecosystems tend to decrease NEP as temperature rises  
293 (**Figure 2**). Additionally, the comparison between model results indicated that the  
294 DGVMs were unable to reproduce several features of the global land C sinks observed  
295 in inversion models. Process-based earth system models will need to improve their  
296 parameterisation to capture these features in order to better predict the future of land C  
297 sinks.

298

299 **References:**

- 300 1. Canadell, J. G. *et al.* Contributions to accelerating atmospheric CO<sub>2</sub> growth from  
301 economic activity, carbon intensity, and efficiency of natural sinks. *Proc. Natl.*  
302 *Acad. Sci. U. S. A.* **104**, 18866–70 (2007).
- 303 2. Le Quéré, C. *et al.* Global Carbon Budget 2017. *Earth Syst. Sci. Data* **10**, 405–  
304 448 (2018).
- 305 3. Ciais, P. *et al.* Europe-wide reduction in primary productivity caused by the heat  
306 and drought in 2003. *Nature* **437**, 529–533 (2005).
- 307 4. Crowther, T. W. *et al.* Quantifying global soil carbon losses in response to  
308 warming. *Nature* **540**, 104–108 (2016).
- 309 5. Fernández-Martínez, M. *et al.* Atmospheric deposition, CO<sub>2</sub>, and change in the  
310 land carbon sink. *Sci. Rep.* **7:9632**, 1–13 (2017).
- 311 6. Peñuelas, J. *et al.* Shifting from a fertilization-dominated to a warming dominated  
312 period. *Nat. Ecol. Evol.* **1**, 1438–1445 (2017).
- 313 7. Ainsworth, E. A. & Long, S. P. What have we learned from 15 years of free-air  
314 CO<sub>2</sub> enrichment (FACE)? A meta-analytic review of the responses of  
315 photosynthesis, canopy properties and plant production to rising CO<sub>2</sub>. *New*  
316 *Phytol.* **165**, 351–71 (2005).
- 317 8. Medlyn, B. E. *et al.* Using ecosystem experiments to improve vegetation models.  
318 *Nat. Clim. Chang.* **5**, 528–534 (2015).
- 319 9. Keenan, T. F. *et al.* Increase in forest water-use efficiency as atmospheric  
320 carbon dioxide concentrations rise. *Nature* **499**, 324–327 (2013).
- 321 10. Alexander, L. *et al.* *Climate Change 2013: The Physical Science Basis -*  
322 *Summary for Policymakers. Fifth Assessment Report* (Intergovernmental Panel  
323 on Climate Change, 2013).
- 324 11. Fernández-Martínez, M. *et al.* Spatial variability and controls over biomass  
325 stocks, carbon fluxes and resource-use efficiencies in forest ecosystems. *Trees,*  
326 *Struct. Funct.* **28**, 597–611 (2014).
- 327 12. Beer, C. *et al.* Terrestrial gross carbon dioxide uptake: global distribution and  
328 covariation with climate. *Science (80-. ).* **329**, 834–8 (2010).

- 329 13. Luysaert, S. *et al.* CO<sub>2</sub> balance of boreal, temperate, and tropical forests  
330 derived from a global database. *Glob. Chang. Biol.* **13**, 2509–2537 (2007).
- 331 14. de Vries, W. & Posch, M. Modelling the impact of nitrogen deposition, climate  
332 change and nutrient limitations on tree carbon sequestration in Europe for the  
333 period 1900–2050. *Environ. Pollut.* **159**, 2289–2299 (2011).
- 334 15. Wamelink, G. W. W. *et al.* Modelling impacts of changes in carbon dioxide  
335 concentration, climate and nitrogen deposition on carbon sequestration by  
336 European forests and forest soils. *For. Ecol. Manage.* **258**, 1794–1805 (2009).
- 337 16. Wamelink, G. W. W. *et al.* Effect of nitrogen deposition reduction on biodiversity  
338 and carbon sequestration. *For. Ecol. Manage.* **258**, 1774–1779 (2009).
- 339 17. de Vries, W., Du, E. & Butterbach-Bahl, K. Short and long-term impacts of  
340 nitrogen deposition on carbon sequestration by forest ecosystems. *Curr. Opin.*  
341 *Environ. Sustain.* **9–10**, 90–104 (2014).
- 342 18. Luysaert, S. *et al.* The European carbon balance. Part 3: forests. *Glob. Chang.*  
343 *Biol.* **16**, 1429–1450 (2010).
- 344 19. Magnani, F. *et al.* The human footprint in the carbon cycle of temperate and  
345 boreal forests. *Nature* **447**, 848–50 (2007).
- 346 20. Thomas, R. B., Spal, S. E., Smith, K. R. & Nippert, J. B. Evidence of recovery of  
347 *Juniperus virginiana* trees from sulfur pollution after the Clean Air Act. *Proc. Natl.*  
348 *Acad. Sci. U. S. A.* **110**, 15319–24 (2013).
- 349 21. Oulehle, F. *et al.* Major changes in forest carbon and nitrogen cycling caused by  
350 declining sulphur deposition. *Glob. Chang. Biol.* **17**, 3115–3129 (2011).
- 351 22. Truog, E. Soil Reaction Influence on Availability of Plant Nutrients<sup>1</sup>. *Soil Sci.*  
352 *Soc. Am. J.* **11**, 305 (1946).
- 353 23. Fernández-Martínez, M. *et al.* Nutrient availability as the key regulator of global  
354 forest carbon balance. *Nat. Clim. Chang.* **4**, 471–476 (2014).
- 355 24. Zhu, Z. *et al.* Greening of the Earth and its drivers. *Nat. Clim. Chang.* **6**, 791–795  
356 (2016).
- 357 25. Chevallier, F. *et al.* CO<sub>2</sub> surface fluxes at grid point scale estimated from a  
358 global 21 year reanalysis of atmospheric measurements. *J. Geophys. Res.* **115**,

- 359 D21307 (2010).
- 360 26. Rödenbeck, C., Houweling, S., Gloor, M. & Heimann, M. CO<sub>2</sub> flux history 1982–  
361 2001 inferred from atmospheric data using a global inversion of atmospheric  
362 transport. *Atmos. Chem. Phys.* **3**, 1919–1964 (2003).
- 363 27. Aber, J. *et al.* Forest Processes and Global Environmental Change: Predicting  
364 the Effects of Individual and Multiple Stressors. *Bioscience* **51**, 735 (2001).
- 365 28. Prentice, I. C., Heimann, M. & Sitch, S. The carbon balance of the terrestrial  
366 biosphere: Ecosystem models and Atmospheric observations. *Ecol. Appl.* **10**,  
367 1553–1573 (2000).
- 368 29. Cheng, L. *et al.* Recent increases in terrestrial carbon uptake at little cost to the  
369 water cycle. *Nat. Commun.* **8**, 110 (2017).
- 370 30. Norby, R. J., Warren, J. M., Iversen, C. M., Medlyn, B. E. & McMurtrie, R. E.  
371 CO<sub>2</sub> enhancement of forest productivity constrained by limited nitrogen  
372 availability. *Proc. Natl. Acad. Sci. U. S. A.* **107**, 19368–73 (2010).
- 373 31. Norby, R. J. *et al.* Forest response to elevated CO<sub>2</sub> is conserved across a broad  
374 range of productivity. *Proc. Natl. Acad. Sci. U. S. A.* **102**, 18052–18056 (2005).
- 375 32. Van Groenigen, K. J. *et al.* The Impact of Elevated Atmospheric CO<sub>2</sub> on Soil C  
376 and N Dynamics. *Ecol. Stud.* **187**, 374–391 (2006).
- 377 33. Terrer, C. *et al.* Mycorrhizal association as a primary control of the CO<sub>2</sub>  
378 fertilization effect. *Science* **353**, 72–4 (2016).
- 379 34. McCarthy, H. R. *et al.* Re-assessment of plant carbon dynamics at the Duke  
380 free-air CO<sub>2</sub> enrichment site: interactions of atmospheric [CO<sub>2</sub>] with nitrogen and  
381 water availability over stand development. *New Phytol.* **185**, 514–528 (2010).
- 382 35. Hyvönen, R. *et al.* The likely impact of elevated [CO<sub>2</sub>], nitrogen deposition,  
383 increased temperature and management on carbon sequestration in temperate  
384 and boreal forest ecosystems: a literature review. *New Phytol.* **173**, 463–80  
385 (2007).
- 386 36. Ryan, M. G. Effects of climate change on plant respiration. *Ecol. Appl.* **1**, 157–  
387 167 (1991).
- 388 37. Amthor, J. S. Scaling CO<sub>2</sub> Photosynthesis Relationships from the Leaf to the

- 389 Canopy. *Photosynth. Res.* **39**, 321–350 (1994).
- 390 38. Wu, Z., Dijkstra, P., Koch, G. W., Peñuelas, J. & Hungate, B. a. Responses of  
391 terrestrial ecosystems to temperature and precipitation change: a meta-analysis  
392 of experimental manipulation. *Glob. Chang. Biol.* **17**, 927–942 (2011).
- 393 39. Chevallier, F. *et al.* Toward robust and consistent regional CO<sub>2</sub> flux estimates  
394 from in situ and spaceborne measurements of atmospheric CO<sub>2</sub>. *Geophys. Res.*  
395 *Lett.* **41**, 1065–1070 (2014).
- 396 40. Olivier, J. G. J. & Berdowski, J. J. M. in *The Climate System* (eds. Berdowski, J.,  
397 Guicherit, R. & Heij, B. J.) 33–78 (2001).
- 398 41. Sitch, S. *et al.* Recent trends and drivers of regional sources and sinks of carbon  
399 dioxide. *Biogeosciences* **12**, 653–679 (2015).
- 400 42. Harris, I., Jones, P. D. D., Osborn, T. J. J. & Lister, D. H. H. Updated high-  
401 resolution grids of monthly climatic observations - the CRU TS3.10 Dataset. *Int.*  
402 *J. Climatol.* **34**, online, update (2013).
- 403 43. Vicente-serrano, S. M., Beguería, S. & López-Moreno, J. I. A Multiscalar Drought  
404 Index Sensitive to Global Warming: The Standardized Precipitation  
405 Evapotranspiration Index. *J. Clim.* **23**, 1696–1718 (2010).
- 406 44. Zuur, A., Ieno, E., Walker, N., Saveliev, A. & Smith, G. *Mixed effects models and*  
407 *extensions in ecology with R.* (Springer science, 2009).
- 408 45. Mathias, J. M. & Thomas, R. B. Disentangling the effects of acidic air pollution,  
409 atmospheric CO<sub>2</sub>, and climate change on recent growth of red spruce trees in  
410 the Central Appalachian Mountains. *Glob. Chang. Biol.* **24**, 3938–3953 (2018).
- 411 46. R Core Team. R: A Language and Environment for Statistical Computing. (2016).
- 412 47. Barton, K. MuMIn: Multi-model inference. R package version 1.17.1.  
413 <http://CRAN.R-project.org/package=MuMIn>. (2015).
- 414 48. Nakagawa, S. & Schielzeth, H. A general and simple method for obtaining R<sup>2</sup>  
415 from generalized linear mixed-effects models. *Methods Ecol. Evol.* **4**, 133–142  
416 (2013).
- 417 49. Breheny, P. & Burchett, W. Visualization of Regression Models Using visreg, R  
418 package version 2.2-0. (2015).

419 **Correspondence and requests for materials should be addressed to:**

420 Marcos Fernández-Martínez: marcos.fernandez-martinez@uantwerpen.be

421 **Acknowledgements**

422 This research was supported by the Spanish Government project CGL2016-79835-P  
423 (FERTWARM), the European Research Council Synergy grant ERC-2013-726 SyG-  
424 610028 IMBALANCE-P, and the Catalan Government project SGR 2017-1005. M.F-M  
425 and S.V. are a postdoctoral fellows of the Research Foundation – Flanders (FWO).  
426 J.G.C. thanks the support of the National Environmental Science Programme ESCC  
427 Hub. We thank Christian Röedenbeck for his advice and for distributing Jena  
428 CarboScope and all the modellers that contributed to the TRENDY project.

429

430 **Author Contributions**

431 M.F-M., J.S., I.A.J., and J.P. conceived, analyzed and wrote the paper. F.C., P.F., and  
432 S.S., provided data. All authors contributed substantially to the writing and discussion of  
433 the paper.

434

435 **Figure captions**

436 **Figure 1: Global trends in NEP and their contributing factors.** Global temporal  
437 contributions of CO<sub>2</sub>, climate and land-use change to the trends in NEP (annual change)  
438 are shown on the right side of each panel. The difference between the modelled temporal  
439 contributions and the trends (shaded) has been treated as an unknown contribution to  
440 the temporal variation in NEP. Statistically significant ( $P < 0.01$ ) temporal variations of  
441 the predictors are shown in square brackets. Error bars indicate 95% confidence  
442 intervals. The boxplots in panel c indicate the estimated contributions of the 10 DVGMS  
443 used in the TRENDY ensemble. Units are ppm y<sup>-1</sup> for CO<sub>2</sub>, °C y<sup>-1</sup> for temperature, mm y<sup>-1</sup>  
444 <sup>2</sup> for precipitation, standard deviation for SPEI, and percentage of land-use cover per  
445 pixel for forests, crops, and urban areas. See the Materials and Methods section for  
446 information about the methodology used to calculate the contributions. Significance  
447 levels: \*,  $P < 0.01$ ; \*\*,  $P < 0.005$ ; \*\*\*,  $P < 0.001$ .

448 **Figure 2: Plots showing the estimated effects of the interactions of the statistical**  
449 **models.** The graphs show interactions between CO<sub>2</sub> and climate (mean annual  
450 precipitation [MAP] and temperature [MAT], and annual anomalies in temperature  
451 [MAT.an]) on NEP for the MACC-II and Jena CarboScope inversion models and the  
452 TRENDY ensemble. Shaded bands indicate the 95% confidence intervals of the slopes.  
453 Non-significant interactions are indicated by “n.s.”.

454 **Table 1: Global and latitudinal analyses of sensitivity of NEP to changes in**  
455 **atmospheric CO<sub>2</sub> concentrations and mean annual temperature.** The “%” columns  
456 indicate the contribution of the latitudinal band to the global estimate. Differences are  
457 calculated as the difference between the sum of all latitudinal bands and the global  
458 estimate. Bold coefficients differ significantly from 0 at the 0.01 level. Empty cells indicate  
459 that anomalies in temperature were not a significant predictor in the models predicting  
460 NEP. Units are Tg C y<sup>-1</sup> ppm<sup>-1</sup> for CO<sub>2</sub> and Tg C y<sup>-1</sup> C<sup>-1</sup> for temperature.

461 **Table 2: Global and latitudinal trends and temporal contributions of changes in**  
462 **atmospheric CO<sub>2</sub> concentrations and mean annual temperature to NEP trends.** The  
463 “%” columns indicate the percentage of contribution of each latitudinal band to the global  
464 estimate. Columns “Cont.” show the percentage of contribution of CO<sub>2</sub> and temperature  
465 to the trends in NEP. Column “Other” shows the difference between the NEP trend and  
466 the sum of contributions of CO<sub>2</sub> and temperature. If different from zero, it indicates that  
467 other factors are contributing to the trends in NEP. The “differences” rows are calculated  
468 as the difference between the sum of all latitudinal bands and the global estimate. NH

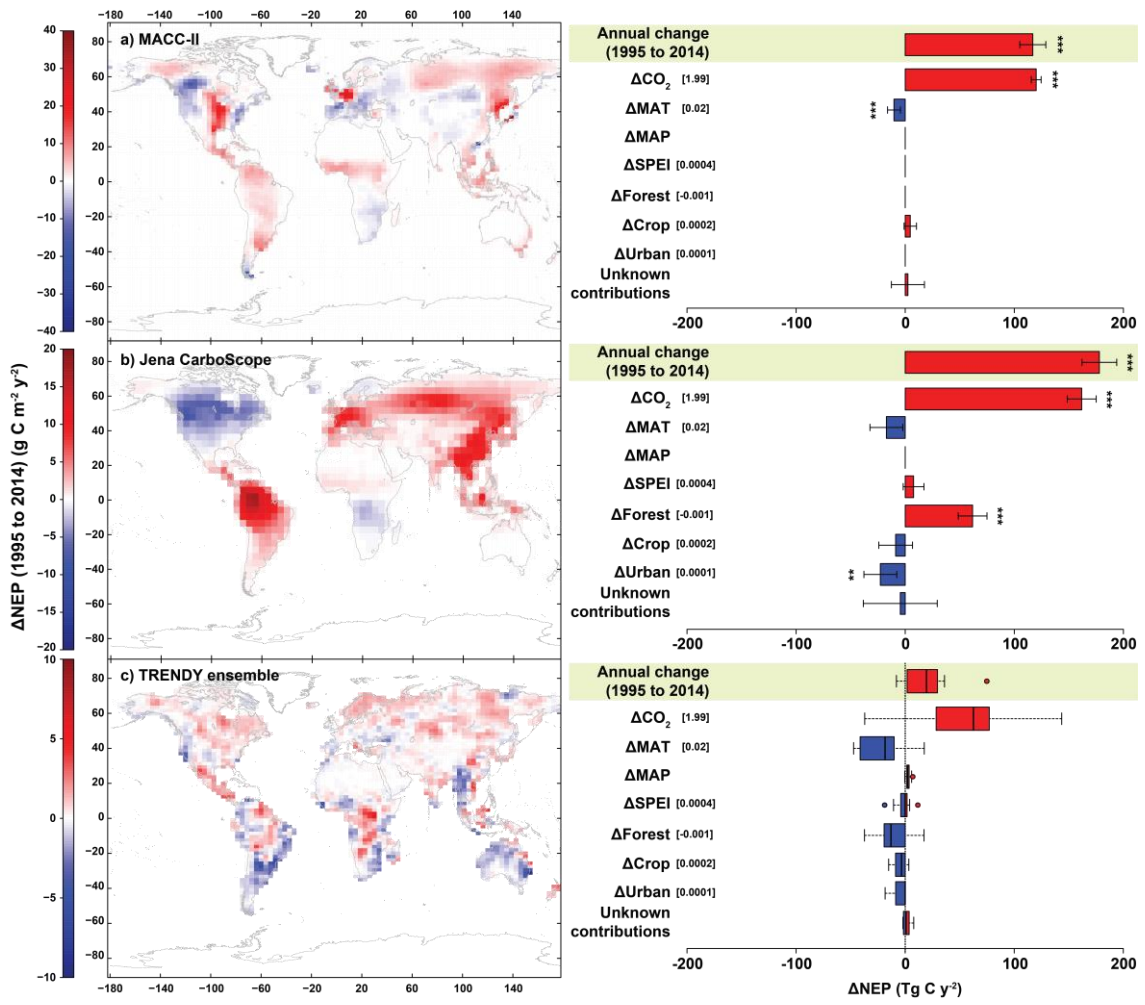
469 and SH indicate Northern and Southern Hemispheres, respectively. Bold coefficients  
470 differ significantly from 0 at the 0.01 level. Empty cells indicate that anomalies in  
471 temperature were not a significant predictor in the models predicting NEP. Units are Tg  
472 C y<sup>-1</sup> for trends, Tg C y<sup>-1</sup> ppm<sup>-1</sup> for CO<sub>2</sub> and Tg C y<sup>-1</sup> C<sup>-1</sup> for temperature. Errors were  
473 calculated using the error propagation method. See the Materials and Methods section  
474 for information about the methods used to calculate the contributions.

475

476

477

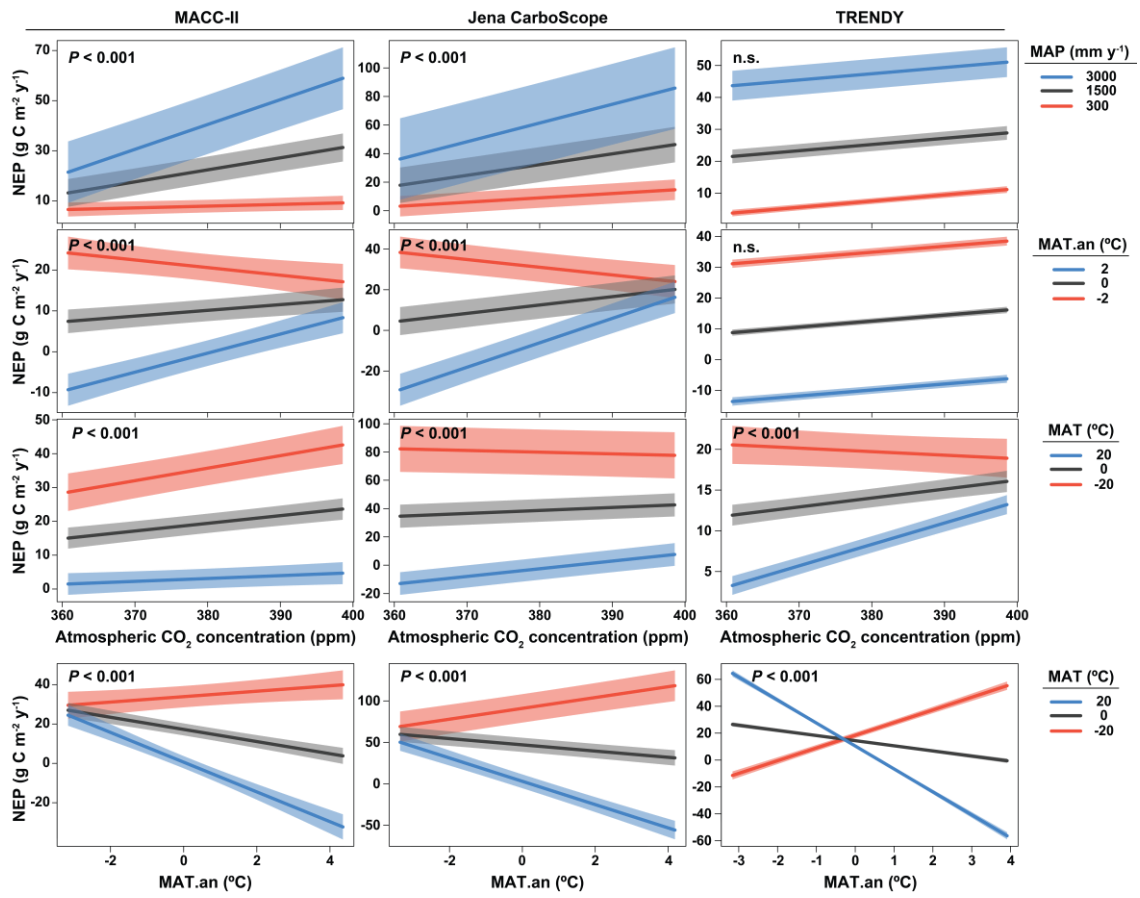
478 **Figure 1**



479

480

481 **Figure 2**



482

483

484 **Table 1**

	CO <sub>2</sub>	%	Temperature	%
<i>MACC</i>				
NH >55°	<b>8.5 ± 0.4</b>	14.1	-35.3 ± 24.1	6.8
NH 35-55°	<b>14.7 ± 1.3</b>	24.3	-132.0 ± 259.9	25.6
NH 15-35°	<b>-5.0 ± 1.4</b>	-8.3		
NH 15-SH 15°	<b>31.9 ± 0.7</b>	52.9	101.9 ± 216.6	-19.8
SH 15-35°	<b>2.2 ± 0.9</b>	3.7	-150.2 ± 131.3	29.1
SH 35-55°	0.6 ± 0.3	1.0	-13.4 ± 49.3	2.6
<b>Global</b>	<b>60.4 ± 1.2</b>		<b>-515.7 ± 152.4</b>	
<b>Difference</b>	<b>-7.4 ± 2.6</b>	-12.3	286.6 ± 397.4	-55.6
<i>JENA</i>				
NH >55°	-0.3 ± 1.0	-0.3	-49.8 ± 48.2	5.8
NH 35-55°	<b>11.1 ± 3.9</b>	13.6	-213.6 ± 558.1	24.9
NH 15-35°	<b>26.3 ± 2.7</b>	32.3	-268.7 ± 400.0	31.3
NH 15-SH 15°	<b>54.2 ± 3.6</b>	66.6	-697.6 ± 1136.5	81.2
SH 15-35°	<b>5.4 ± 0.9</b>	6.6	-167.0 ± 133.9	19.4
SH 35-55°	<b>0.2 ± 0.0</b>	0.3		
<b>Global</b>	<b>81.4 ± 3.4</b>		<b>-859.2 ± 386.3</b>	
<b>Difference</b>	15.4 ± 6.9	19.0	-537.4 ± 1390.2	62.5
<i>TRENDY</i>				
NH >55°	<b>2.8 ± 0.1</b>	9.0	<b>17.3 ± 7.3</b>	-1.6
NH 35-55°	<b>5.8 ± 0.5</b>	19.0	<b>-251.1 ± 79.3</b>	23.1
NH 15-35°	<b>5.9 ± 0.6</b>	19.4	<b>-368.8 ± 51.9</b>	33.9
NH 15-SH 15°	<b>16.6 ± 1.1</b>	54.2	<b>-1612.2 ± 213.4</b>	148.2
SH 15-35°	<b>4.6 ± 1.2</b>	14.9	<b>-379.2 ± 141.1</b>	34.9
SH 35-55°	0.3 ± 0.2	1.0	-36.8 ± 18.1	3.4
<b>Global</b>	<b>30.7 ± 1.2</b>		<b>-1088.0 ± 118.1</b>	
<b>Difference</b>	<b>5.4 ± 2.1</b>	17.5	<b>-1542.7 ± 298.0</b>	141.8

	Trends	%	CO <sub>2</sub>	%	Cont	Temp	%	Cont.	Other
<i>MACC</i>									
NH >55°	20.1 ± 1.2	17.2	17.0 ± 0.8	14.1	84.4	-1.2 ± 0.8	11.5	-5.9	4.3 ± 1.7
NH 35-55°	17.5 ± 5.0	15.0	29.2 ± 2.7	24.3	166.6	-1.7 ± 3.2	16.1	-9.4	-10.0 ± 6.5
NH 15-35°	14.0 ± 3.1	12.0	-9.9 ± 2.8	-8.3	-71.0			0.0	23.9 ± 4.1
NH 15-SH 15°	55.4 ± 2.7	47.4	63.5 ± 1.5	52.9	114.6	0.9 ± 1.9	-8.9	1.6	-9.0 ± 3.6
SH 15-35°	7.6 ± 1.4	6.5	4.4 ± 1.9	3.7	57.6	-2.3 ± 2.0	22.2	-29.8	5.5 ± 3.1
SH 35-55°	2.3 ± 0.6	2.0	1.2 ± 0.7	1.0	49.9	-0.3 ± 1.0	2.5	-11.2	1.4 ± 1.3
Global	116.9 ± 6.1		120.1 ± 2.3		102.7	-10.3 ± 3.0		-8.8	7.1 ± 7.2
Difference	0.0 ± 9.1	0.0	-14.8 ± 5.2	-12.3		5.8 ± 5.4	-56.6		
<i>JENA</i>									
NH >55°	13.8 ± 2.2	7.7	-0.5 ± 2.1	-0.3	-3.8	-1.7 ± 1.7	9.9	-12.4	16.0 ± 3.5
NH 35-55°	49.8 ± 5.9	28.0	22.0 ± 7.7	13.6	44.1	-2.7 ± 6.9	15.4	-5.3	30.5 ± 11.9
NH 15-35°	49.2 ± 4.0	27.6	52.3 ± 5.3	32.3	106.2	-5.0 ± 7.4	29.0	-10.2	1.9 ± 10.0
NH 15-SH 15°	80.4 ± 5.1	45.2	107.7 ± 7.1	66.6	133.9	-5.7 ± 9.2	32.9	-7.0	-21.6 ± 12.7
SH 15-35°	10.4 ± 1.3	5.8	10.7 ± 1.7	6.6	103.1	-2.8 ± 2.2	16.2	-26.9	2.5 ± 3.1
SH 35-55°	0.5 ± 0.1	0.3	0.4 ± 0.1	0.3	87.2				0.1 ± 0.1
Global	178.0 ± 8.1		161.8 ± 6.8		90.9	-17.2 ± 7.7		-9.7	33.4 ± 13.1
Difference	26.1 ± 12.2	14.7	30.7 ± 13.8	19.0		-0.6 ± 16.0	3.4		
<i>TRENDY</i>									
NH >55°	9.3 ± 0.6	41.4	5.5 ± 0.3	9.0	59.0	0.6 ± 0.2	-2.7	6.1	3.3 ± 0.7
NH 35-55°	9.4 ± 1.3	41.5	11.6 ± 0.9	19.0	124.0	-3.0 ± 0.9	13.9	-31.6	0.7 ± 1.8
NH 15-35°	3.3 ± 1.3	14.9	11.8 ± 1.1	19.4	352.9	-7.9 ± 1.0	36.9	235.0	-0.6 ± 2.0
NH 15-SH 15°	10.1 ± 2.3	45.0	33.0 ± 2.1	54.2	326.2	-17.2 ± 1.8	80.8	170.2	-5.7 ± 3.6
SH 15-35°	-13.7 ± 1.8	-60.9	0.5 ± 0.1	0.9	-3.8	-0.3 ± 0.1	1.6	2.5	-13.9 ± 1.8
SH 35-55°	-1.0 ± 0.4	-4.7	0.6 ± 0.5	1.0	-55.4	-0.7 ± 0.4	3.5	70.4	-0.9 ± 0.7
Global	22.5 ± 3.1		61.0 ± 2.5		270.7	-21.3 ± 2.2		-94.7	-17.1 ± 4.5
Difference	-5.2 ± 4.7	-22.9	2.1 ± 3.6	3.4		-7.3 ± 3.2	34.0		

487

488

## 489 **Methods**

### 490 Datasets

#### 491 *NEP data*

492 We used gridded global monthly NEP data for 1995–2014 from two inversion models: i)  
493 the MACC (Monitoring Atmospheric Composition and Climate) CO<sub>2</sub> ([http://www.gmes-  
494 atmosphere.eu/catalogue/](http://www.gmes-atmosphere.eu/catalogue/))<sup>25,39</sup> database, version v14r2 and ii) the Jena CarboScope  
495 database version s93\_v3.7 using a constant network of towers ([http://www.bgc-  
496 jena.mpg.de/CarboScope/](http://www.bgc-jena.mpg.de/CarboScope/))<sup>26</sup>. The MACC CO<sub>2</sub> atmospheric inversion system relies on  
497 the variational formulation of Bayes' theorem to analyse direct measurements of CO<sub>2</sub>  
498 concentrations from 130 sites around the globe for 1979-2014. Optimised fluxes were  
499 calculated at a global horizontal resolution of 3.75 × 1.875° (longitude, latitude) and a  
500 temporal resolution of eight days, separately for daytime and night-time. The underlying  
501 transport model was run with interannually varying meteorological data from the ECMWF  
502 ERA-Interim reanalysis. The Jena inversion model estimates the interannual variability  
503 of CO<sub>2</sub> fluxes based on raw CO<sub>2</sub> concentration data from 50 sites. The model uses a  
504 variational approach with the TM3 transport model (4 × 5°, using interannually varying  
505 winds). Prior terrestrial fluxes were obtained from a modelled mean biospheric pattern  
506 and fossil-fuel emissions from the EDGAR emission database<sup>40</sup>. We also used NEP data  
507 from an ensemble of 10 dynamic global vegetation models (DGVMs) compiled by the  
508 TRENDY project (version 4, models CLM4.5, ISAM, JSBACH, JULES, LPJG, LPX, OCN,  
509 ORCHIDEE, VEGAS, and VISIT) to see if results obtained from atmospheric inversions  
510 data match those obtained with DGVMs simulations<sup>41</sup>. We used the output from  
511 simulation experiment S3, which was run with varying atmospheric CO<sub>2</sub> and changing  
512 land use and climate<sup>41</sup>.

#### 513 *Meteorological, land-use change and atmospheric CO<sub>2</sub> data*

514 We extracted gridded temperature and precipitation time series from the Climatic  
515 Research Unit TS3.23 dataset<sup>42</sup>. We also used the SPEI (Standardised Precipitation-  
516 Evapotranspiration Index) drought index<sup>43</sup> from the global SPEI database  
517 (<http://SPEI.csic.es/database.html>) as a measure of drought intensity (positive values  
518 indicate wetter than average meteorological conditions, negative values indicate drier  
519 than average conditions). We used annual SPEI1 (monthly SPEI averaged over a year).  
520 Mean annual temperature (MAT) and precipitation (MAP) and SPEI were calculated for  
521 each year and pixel. We used land-use change maps from land-use harmonisation<sup>2</sup>  
522 (LUH2, <http://luh.umd.edu/data.shtml>) and calculated the percent coverages of forests,

523 croplands, and urban areas per pixel, so we could further estimate whether they  
524 increased or decreased from 1995 to 2014. We used the data for atmospheric CO<sub>2</sub>  
525 concentration from Mauna Loa Observatory provided by the Scripps Institution of  
526 Oceanography (Scripps CO<sub>2</sub> programme).

#### 527 *Data for N and S deposition*

528 Annual data for N (oxidised N [N<sub>OX</sub>] from NO<sub>3</sub><sup>-</sup> and reduced N [N<sub>RED</sub>] from NH<sub>4</sub><sup>+</sup>) and S  
529 (SO<sub>4</sub><sup>-</sup>) wet deposition were extracted from: i) the European Monitoring and Evaluation  
530 Programme (EMEP) with a spatial resolution of 0.15 × 0.15° for longitude and latitude,  
531 ii) the MSC-W chemical-transport model developed to estimate regional atmospheric  
532 dispersion and deposition of acidifying and eutrophying N and S compounds over  
533 Europe, and iii) the National Atmospheric Deposition Program (NADP) covering the USA  
534 with a spatial resolution of 0.027 × 0.027° for longitude and latitude. We used only data  
535 for wet deposition because the NADP database only contained records for dry deposition  
536 for 2000. Analyses focused on atmospheric deposition and were restricted to Europe  
537 and the USA because temporal gridded maps of atmospheric deposition were not  
538 available for other regions. Maps of atmospheric deposition for the regional analyses  
539 were adjusted to the resolution of the C-flux maps (3.75 × 1.875° for the MACC-II model  
540 and 4 × 5° for the Jena CarboScope model for longitude and latitude).

#### 541 Statistical analyses

##### 542 *Gridded, global and regional trend detection on NEP*

543 To determine how NEP has changed from 1995 to 2014, we first calculated the trends  
544 for each pixel in both inversion models and an average dataset of the TRENDY ensemble  
545 using linear regressions with an autoregressive and moving-average (ARMA)  
546 (autoregressive structure at lag p=1, and no moving average q=0) correlation structure  
547 to account for temporal autocorrelation. Trends over larger areas (e.g. the entire world,  
548 latitudinal bands), either for NEP or the predictor variables, were calculated using  
549 generalised linear mixed models (GLMMs) with random slopes, including also random  
550 intercepts<sup>44</sup> (e.g. NEP ~ year). We used pixel as the random factor (affecting the  
551 intercepts and slopes of the year), and an ARMA (p=1, q=0) correlation structure. All  
552 average trends shown were calculated using this methodology.

##### 553 *Calculation of temporal contributions on trends of NEP*

554 The temporal contributions of increasing CO<sub>2</sub>, climate (MAT, MAP, and SPEI), and land-  
555 use change (forests, croplands, and urban areas) to the observed trends in NEP were

556 assessed for the MACC-II, Jena CarboScope, and TRENDY datasets for the entire  
557 world. We repeated the analysis for five latitudinal bands to determine if the contributions  
558 of CO<sub>2</sub>, climate, and land-use change were globally consistent using MACC-II, Jena  
559 CarboScope, and the mean ensemble of the TRENDY datasets. For the MACC-II and  
560 Jena CarboScope datasets, we also determined the temporal contribution of  
561 atmospheric deposition of N (N<sub>OX</sub> and N<sub>RED</sub>) and S to the trends in NEP in a combined  
562 analysis that also included CO<sub>2</sub>, climatic, and land-use trends. This latter analysis was  
563 restricted to Europe and the USA due to the lack of atmospheric-deposition time series  
564 for the rest of the world.

565 The temporal contributions of the predictor variables were calculated following the  
566 methodology established in references<sup>5,45</sup>, as follows:

567 i) using a GLMM with an autocorrelation structure for lag 1 (AR1) and using the pixel as  
568 the random factor affecting only the intercept, we fitted full models for NEP as a function  
569 of CO<sub>2</sub>, mean MAT per pixel, annual anomaly of MAT, mean MAP per pixel, annual  
570 anomaly of MAP, the annual SPEI, and mean percentage of forested, cropped, and  
571 urban areas per pixel and their annual anomalies. We included the first-order interaction  
572 terms between CO<sub>2</sub> and all predictors and between the mean values and the anomalies  
573 for all predictors (except SPEI, which interacted with mean MAT and MAP). When the  
574 interaction term between the means and the anomalies (e.g. MAT mean × MAT anomaly)  
575 was included, the model estimated the effect of the anomaly as a function of the average  
576 value. This implies a change in the effect of increasing or decreasing the anomalies,  
577 depending on the mean for the site (e.g. increasing temperature may have a positive  
578 effect in cold climates but a negative effect in warmer climates). For models including  
579 atmospheric deposition, we also included the interaction between climatic variables and  
580 CO<sub>2</sub> and the interactions between the means and the annual anomalies of atmospheric  
581 deposition (N<sub>OX</sub>, N<sub>RED</sub>, and S). The models were fitted using maximum likelihood to allow  
582 the comparison of models with different fixed factors.

583 ii) We used the stepwise backwards-forwards model selection (*stepAIC* function in R<sup>46</sup>)  
584 from the full models, using the lowest Bayesian information criterion (BIC), to obtain the  
585 best model. The amount of the variance explained by the models was assessed using  
586 the *r.squaredGLMM* function in R (MuMIn package: <sup>47</sup>) following the method of  
587 Nakagawa and Schielzeth (2013). Model residuals met the assumptions required in all  
588 analyses (normality and homoscedasticity of residuals).

589 iii) We then used the selected models to predict the changes of the response variables  
590 during the study period (1995–2014). We first extracted the observed trend (mean  $\pm$   
591 SEM, standard error of the mean) in NEP using raw data with GLMMs with an AR1  
592 autocorrelation structure. We then calculated the trend of NEP predicted by the final  
593 model and the trends of NEP predicted by the same model while maintaining the  
594 temporally varying predictors (i.e., anomalies) constant one at a time (e.g. MAT  
595 anomalies were held constant using the median per pixel, while all other predictors  
596 changed based on the observations). The difference between the predictions for the final  
597 model and when one predictor was controlled was assumed to be the contribution of that  
598 predictor variable to the change in NEP. The differences between all individual  
599 contributions and the observed trend in NEP were treated as unknown contributions.

#### 600 *Calculation of sensitivities of NEP to temporal predictors*

601 Finally, we calculated the average sensitivities of NEP to the predictor changes by  
602 dividing the temporal contributions of each predictor of delta NEP by their temporal  
603 trends. Spatial variability on the effects of temporal predictors to NEP were assessed  
604 using the GLMMs fitted to estimate the temporal contributions of the predictors. To  
605 visualise the interactions we used the R package visreg<sup>49</sup>. All errors were calculated  
606 using the error-propagation method using the following two equations, for additions and  
607 subtractions:  $\epsilon C = \sqrt{(\epsilon A)^2 + (\epsilon B)^2}$ ; and for multiplications and divisions:  $\epsilon C =$   
608  $C \sqrt{\left(\frac{\epsilon A}{A}\right)^2 + \left(\frac{\epsilon B}{B}\right)^2}$ ; where  $\epsilon$  indicates the error associated to each value (A, B or C). To  
609 calculate global and regional estimates we multiplied the model outputs, in units of gC  
610 m<sup>-2</sup>, times land area. We considered the land Earth surface area to be 134375000 km<sup>2</sup>  
611 excluding the Antarctic region. Land area for the different latitudinal bands used were:  
612 >55° N, 23818000 km<sup>2</sup>; 35 to 55° N, 31765000 km<sup>2</sup>; 15 to 35° N, 29213000 km<sup>2</sup>; 15° S  
613 to 15° N, 29926000 km<sup>2</sup>; 15 to 35° S, 17308000 km<sup>2</sup>; and 35 to 55° S, 2345600 km<sup>2</sup>.

614

#### 615 **Data availability**

616 The authors declare that the data supporting the findings of this study are publically  
617 available in the webpages provided in the article. The TRENDY simulations are available  
618 from the corresponding author upon request.

619